

# Numerical Investigation of Bio-inspired Heat Sink Model with Multiple Outlets for Cooling Rectangular Shaped Electronic Circuits

K. Kandassamy<sup>1,\*</sup>, B. Prabu<sup>2</sup>

<sup>1</sup>Department of Mechanical Engineering, Annamalai University, Chidambaram-608002, India

<sup>2</sup>Department of Mechanical Engineering, Pondicherry Engineering College, Puducherry-600001, India

\*Corresponding author email: kandassamy@yahoo.com, Tel.: +91 9486366126

## ABSTRACT

Cooling of electronic circuits is a necessity to ensure reliability and optimum working conditions. In this work a bio-inspired single-inlet flow field having leaf-type branching secondary micro-channel arrays, with aspect ratios 4.3, 8.6 and 12.9 is analyzed. The simulation of the heat sink models is done using finite element based software. The coupling between heat transfer and laminar fluid flow is done using conjugate heat transfer. The heat sinks are subjected to a constant heat flux input and tested for pressure drop of 0.2-0.3 MPa. Validation of simulation results is done by comparing the mixing cup temperature with that obtained by heat balance. The results prove that, bio-inspired model has a low variation in chip surface temperature than traditional micro-channel arrays. Higher aspect ratio models have higher Nusselt numbers for similar pressure drops. The heat sink models with aspect ratio 12.9 at an input pressure 0.3 MPa shows a thermal resistance of 0.126 C/W with pumping power -2.39W.

**Keywords** – Heat sink, Hydraulic Resistance, Micro-channel, Reynolds number, Thermal Resistance.

## 1. INTRODUCTION

Heat sinks are required to dissipate heat fluxes in the range, 1-10M W/m<sup>2</sup> from electronic circuits. As the density of electronic devices per chip increases the heat dissipation also increases. Straight micro channels incur high parasitic power consumption due to higher pressure drops incurred for the power dissipated [1]. Hence it is necessary to find new ways to increase heat-sinking by designing new flow field models that strike a balance between heat transfer and pressure drop. One of the method is to mimic biological flow distribution systems as in the proposed heat sink model. The majorities of the coolants used in heat sinks are air and water [2]. Straight micro channel heat sinks have decreasing temperature gradient in the flow direction due to saturation of fluid thermal capacity, with higher heat transfer rates in the entrance and reduced values near the exit [3]. The split-flow arrangement is recommended in [4] for reduction in flow length,  $\Delta p$  reduction and heat transfer coefficient enhancement. The optimum  $\alpha$  recommended in [5] is 8.8-11.4. Biological designs are achieved in nature by variation in branching channel diameters from inlet to outlet. Most of the bio-inspired flow fields encountered in literature are applied in the field of Proton Exchange Membrane fuel cells [6-12]. Arbabi [13] has given a combination

of conventional and bio-inspired flow fields in their models. Lung and leaf inspired models have shorter path lengths, uniform species and velocity distribution for large number of parallel and high  $\alpha$  channels than ones with longer pathways. Farzaneh et al. [14] uses a square-shaped heat sink flow-fields based on the constructal theory, for a temperature and  $\Delta p$  reduction of 10-20% and- 25-33% respectively in comparison to flow-fields without branches. Parallel micro-channel networks with bio-inspired inlet and outlet manifolds are found [15] to have more surface area, lower  $\Delta p$ , higher C.O.P and ease of manufacturing compared to constructal networks. The angle of the branching channels with the main supply and collecting channels is maintained at 90° as the lower angle branching channels are not able to achieve uniform flow in diagonal corners of the flow field [16]. The reduction in main channel cross section increases  $R_{hy}$  forcing fluid in low resistance branching channels giving a uniform velocity field. The supply and collecting channel dimensions are similar and their angles are determined by trial and error to minimize base surface temperature. Recent processors like AMD's 2990WX [17] are of rectangular cross-section ( $4.411 \times 10^{-3} \text{m}^2$ ), with a Thermal Design Power -TDP of 250W, dissipating a heat flux of 56700 W/m<sup>2</sup>. The  $R_{th}$  requirement for the processor is 0.152 C/W at a maximum operating

temperature of 68C. From the survey of literature, it is obvious that application of bio-inspired flow fields are not experimented or analyzed for application in the field of heat sinking.

Hence this numerical study is conducted to identify a promising flow field pattern. The performance is compared against literature, and applicability of the new bio-inspired flow fields is gauged by their ability to decrease  $\Delta p$  across the flow field, Uniformity of Chip Surface Temperature (UCST),  $R_{hy}$  and  $R_{th}$ .

## 2. ASSUMPTIONS AND BOUNDARY CONDITIONS

The following assumptions are applicable to the finite element models analyzed in this simulation:

- Laminar- incompressible, steady, and single phase flow.
- The solid and fluid properties are temperature dependent.
- The Buoyancy force due to temperature changes is included.
- All external surfaces outside the heat sink are insulated except the bottom plate.
- Heat input to the fluid is the sum of contribution from both base plate and fin lateral surfaces.

The following boundary conditions are used:

- The  $\Delta p$  for the flow fields is maintained at 0.2-0.3MPa. The Re in this analysis does not undergo transition.
- The single-inlet models are analyzed at aspect ratios 4.3; 8.6; 12.9 by varying the flow field height.
- The inlet flow field temperature is maintained at 303K for all the models.
- The buoyancy due to temperature rise is included in the momentum equation as a volumetric source term acting in the Z axis direction.
- Non slip boundary condition is considered for fluid flow.
- The base plate of all the models is heated by a constant heat flux.
- The top plate is insulated and heat is evacuated only through circulating fluid. Radiation heat transfer is neglected.

## 3. GEOMETRICAL AND OPERATIONAL PARAMETERS

The general schematic and operational parameters are given in Figure 1 and Table 1. The models are analyzed at different  $\alpha$ , constant fin pitch and inlet pressure conditions. This is done to study the effect of  $\alpha$  on  $R_{th}$  and  $R_{hy}$ . The material properties are given to the models from the COMSOL in-built material library. Liquid water, Crystalline Silicon, and Poly-dimethyl-siloxane (PDMS) top cover insulation are the materials used in the models. All the fluid properties are given as temperature dependent polynomial functions in the material libraries [18], and the same is used in the models. The models are built on an X-Y plane with all extrusions in the Z direction. The properties of water at 303K are  $\rho$ -997.5 kg/m<sup>3</sup>,  $C_p$ -4180 J/kgK,  $\mu$  -0.001003 kg/ms,  $k_f$  -0.6129 W/mK; properties of crystalline silicon are  $\rho$ -2329 kg/m<sup>3</sup>,  $C_p$ -700 J/kgK,  $\alpha_{th}$ -2.6E-06 1/K,  $k_s$ -130 W/mK; properties of PDMS are  $\rho$ -970 kg/m<sup>3</sup>,  $C_p$ -1460 J/kgK,  $\alpha_{th}$ -9 E-04 1/K,  $k_s$ -0.16 W/mK respectively  $\square$ .

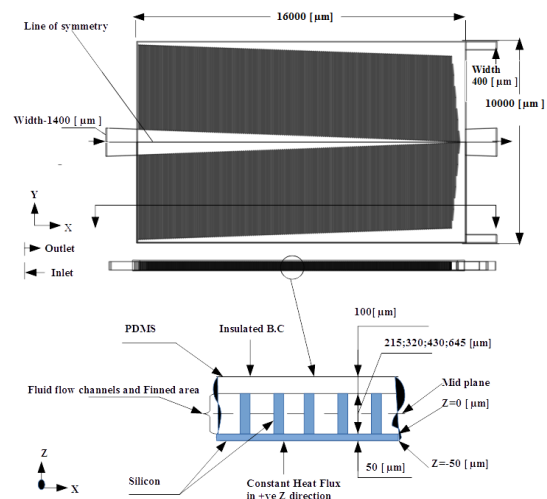


Fig. 1 Basic dimensions of models taken for study

Table 1 Geometrical and operational parameters of the models

Model Parameters	Value
Bottom plate thickness in negative Z axis- $\mu\text{m}$	50
Top cover plate thickness in Z axis - $\mu\text{m}$	100
Cross sectional area of the setup in X-Y plane- $\text{m}^2$	$1.6 \times 10^{-4}$
Inlet temperature of the fluid -K	303
The outlet pressure condition -bar	0
Channel Width - $\alpha$ =4.3;6.4;8.6;12.9	50

#### 4. GOVERNING EQUATIONS AND DATA REDUCTION

The following are the governing equations applicable to all models investigated in this work [18]. The continuity equation is given by equation (1),

$$\rho \nabla \cdot (u) = 0 \tag{1}$$

The momentum is given by equation (2),

$$\rho (u \cdot \nabla) u = \nabla \cdot [-pI + \mu (\nabla u + (\nabla u)^T)] + F \tag{2}$$

where F is the body force term,  $F = -g \cdot \Delta \rho$  (3)

and  $\Delta \rho$  represents the change in density due to thermal heating. The pin fin heat sinks are oriented towards the positive Z direction and gravity vector is positive in the negative Z direction. Due to this the term ‘g’ gets negative sign in the body force term F. The fluid and solid energy is computed using equations (4-5).

$$\rho C_p u \cdot \nabla T + \nabla \cdot q = Q \tag{4}$$

where Q is the heat sinking value per unit volume of the heat sink  $W/m^3$ . The heat supplied to the base- $Q_{th}$  equals the sum of heat carried by fluid from base, heat carried by fluid from fins and heat stored in solid. The conduction equation (5) is applicable to solid and fluid regions,

$$q = -k \nabla T \tag{5}$$

The overall Nu and inlet Re are calculated using equations (6-7) based on the inlet  $D_{h-in}$ .

$$Nu = \frac{h_{avg} D_{h-in}}{k_f} \tag{6}$$

where  $h_{avg}$  is the overall heat transfer coefficient calculated based on the inlet to outlet temperature change of the coolant fluid. The Channel Re is calculated by evaluating the average velocity and kinematic viscosity from the simulation results at mid-channel height and multiplying with the  $D_h$ . The inlet Re is calculated using equation (7),

$$Re_{in} = \frac{\rho u D_{h-in}}{\mu} \tag{7}$$

The  $R_{th}$  and  $R_{hy}$  for the models are calculated using equations (8-11),

$$R_{th} = \frac{T_{max} - T_{min}}{Q_{th}} \tag{8}$$

where  $Q_{th} = q_b \cdot A_b$  (9)

$T_{max}$  is the maximum base plate temperature near the outlet and  $T_{min}$  is the inlet fluid temperature,

$$R_{hy} = \frac{\Delta p}{Q_{hy}} \text{ Pa s/m}^3 \tag{10}$$

where  $Q_{hy} = u_{in} \cdot A_{in} \text{ m}^3/\text{s}$  (11)

The overall heat transfer coefficient is calculated using equation (12),

$$h_{avg} = \frac{q_b}{T_{max} - T_{min}} \text{ W/m}^2 \text{ K} \tag{12}$$

where  $q_b$  is the heat flux applied to the base plate of heat sink ( $W/m^2$ ). The total heat flux magnitude from base and fin surfaces is calculated using equation (13),

$$q = Q_{convection} + Q_{conduction} \text{ W/m}^2 \tag{13}$$

The uniformity of the base surface temperature is calculated using equation (14),

$$UCST (\%) = \frac{T_{b,max} - T_{b,min}}{T_{b,avg}} \tag{14}$$

The pumping power is calculated using equation (15),

$$W_p = u_{in} \cdot A_{in} \cdot \Delta p_{avg} \tag{15}$$

A numerical performance index PF is defined similar to references [15, 19], as the ratio of heat-sinking to the pumping work. A design with a higher PF is capable of dissipating more heat for a given pumping power. The temperature difference is included, to factor in the effect of its non-uniformity, and is computed using equation (16),

$$PF = Q_{th} / (T_{b,max} - T_{b,min}) \cdot W_p \text{ 1/K} \tag{16}$$

The Po for the various flow-fields are calculated using the correlation (17), developed by Shah and London as referred from [19]. The friction factor-fr is evaluated using the relation (18).

$$Po = 24(1 - 1.3553/\alpha + 1.9467/\alpha^2 - 1.7012/\alpha^3 + 0.9564/\alpha^4 - 0.2537/\alpha^5) \tag{17}$$

$$fr = Po / Re_{ch} \tag{18}$$

#### 5. NUMERICAL ANALYSIS

All the models in this work are solved as full 3D models at lower mesh densities and are split into half

models based on symmetry on a desktop computer using i7-4930k processor and 64GB in-built RAM. The temperature parameters are evaluated at Z=0 as it is the first plane of contact of the fluid with the heat flux, and the flow field parameters are evaluated at mid plane, where  $u_{max}$  is achieved for a fully developed flow.

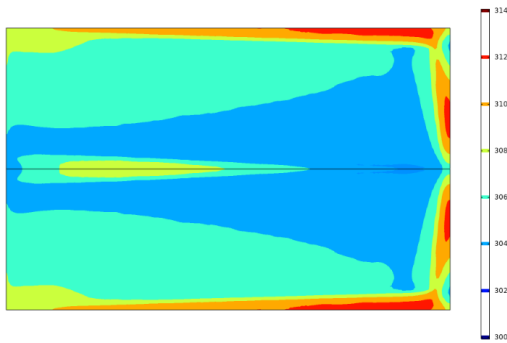


Fig. 2 Temperature contours in K at Z -0 μm

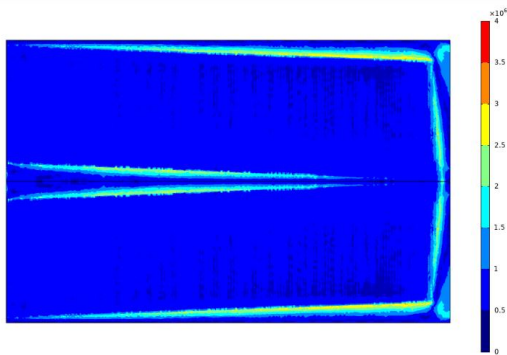


Fig. 3 Heat flux contours in W/m<sup>2</sup> at Z -0 μm

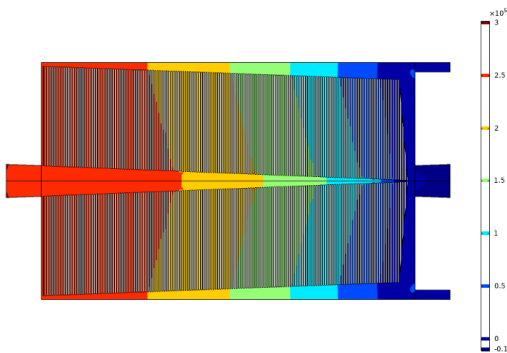


Fig. 4 Pressure contours in Pa at Z -322.5 μm

In the simulation results analyzed here, the base temperature of the flow field at Z=0 [Fig. 2], the mid-plane velocity magnitude of the flow field [Fig. 4], the pressure contours from inlet to outlet [Fig. 5], and the total heat flux magnitude at mid-plane [Fig. 3] for model with  $\alpha$ -12.9 and  $\Delta p$ -0.3Mpa are presented. The grid independence test is done for the models by

increasing the grid density until the change in the maximum temperature of the base plate-  $(T_i - T_{i-1})/T_i$  % and the average of the inlet pressure-  $(\Delta p_i - \Delta p_{i-1})/\Delta p_i$  % becomes smaller.

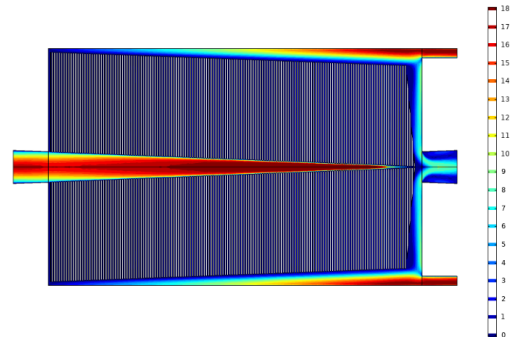


Fig. 5 Velocity contours in m/s at Z -322.5 μm

## 6. RESULT AND DISCUSSION

### 6.1 Theoretical Validation

As the bio-inspired models proposed in this work is a novel, similar model to be used as reference benchmarks are currently unavailable in literature. Hence the validation of the simulation is done by energy balance. The average temperature of the outlet fluid calculated using the energy balance equation (19), and the results of the actual simulation results are tabulated in Table 2.

$$\rho_f \cdot u_{in} \cdot A_{in} \cdot C_{pf} \cdot (T_{avg-out-theo} - T_{avg-in}) = Q_{th} \quad (19)$$

where  $T_{avg-in}$ -303 K and  $T_{avg-out-theo}$  is calculated. The  $C_{pf}$  value is assumed as 4180 J/kgK in the operating temperature range. The weighted average outlet temperature at the outlet obtained by simulation-  $T_{avg-out-act}$  is given by equation (20), where, n- normal vector; T -Temperature; A-Area, u- velocity perpendicular to the outlet plane. The comparison between the calculated value ( $T_{avg-out-theo}$ ) and the weighted average outlet temperature ( $T_{avg-out-act}$ ) in Table 3 shows negligible error.

$$T_{avg-out-act} = \frac{\int T u \cdot ndA}{\int u \cdot ndA} \quad (20)$$

### 6.2 Thermal Characteristics

The analyzed models are tested with heat flux of 0.5 MW/m<sup>2</sup>. The maximum base temperature is lower for high inlet pressures due to higher inlet velocities for a

given flow field. In the model shown in Fig. 1, the temperature rise reaches the maximum value at the outlet manifolds due to adverse temperature gradient. Fig. 2 highlights the flow distribution pattern of the models with near uniform velocity as fluid moves towards the outlets. The fluid flow velocity along the flow channels show a clear uniform flow in the increasing order of velocity magnitude according to inlet pressure. For the same geometric parameters, increase in inlet pressure and  $\alpha$  decreases UCST. The reason for variation is, higher heat fluxes increase non-uniformity in chip temperature, by decreasing temperature gradient of fluid from inlet to outlet. The lowest UCST obtained in this paper is 3.06% [Table 3]. The  $R_{th}$  is the basis for comparing heat transfer performance of heat sinks as shown in Table 4. Increase in  $\alpha$  and inlet pressure decreases  $R_{th}$ . For comparison with [20] all the models are tested at inlet pressure of 206.84 kPa and the heat sink model achieved a  $R_{th}$  of 0.126 C/W as shown in Table 4. For models with lower  $R_{th}$  the PF decreases with increase in  $\alpha$ , indicating higher  $W_p$  necessary. The overall Nu increases with  $\alpha$  and inlet pressure. The Nu values are shown in Table 5.

Table 2 Validation of heat sink models by heat balance

$\Delta p$ kPa	$\alpha$	$Q_{in}$ W	$T_{avg-out-theo}$ K	$T_{avg-out-act}$ K	Error %
206.84	4.3	80	310.2	309.16	-0.33
206.84	6.4	80	307.7	308.39	0.22
206.84	8.6	80	306.4	306.04	-0.11
206.84	12.9	80	305.2	304.96	-0.08
300.00	4.3	80	308.83	307.92	-0.29
300.00	6.4	80	306.8	307.80	0.32
300.00	8.6	80	305.7	305.48	-0.07
300.00	12.9	80	304.8	304.96	0.05

### 6.3 Pressure Drop

The  $\Delta p$  is higher for the analyzed models due to the 90° branching angles of the bio-inspired flow field. In tests conducted with lower angled branching channels similar to surveyed literature [9, 13], show large bypassing of fluid in individual channels nearer to the flow field inlets. The  $R_{hy}$  is a measure of the  $\Delta p$  sustained for maintaining a particular flow rate.

Table 3 UCST for flow fields

Model	$\alpha$	$\Delta p$ kPa	$T_{max}$ K	$T_{min}$ K	$T_{avg}$ K	UCST %
[20]	6.4	206.84	367	296	331.5	21.4
Present Work	4.3	206.84	319.8	304.1	310.2	5.05
	6.4	206.84	316.6	303.9	308.4	4.10
	8.6	206.84	315.2	303.8	307.6	3.70
	12.9	206.84	314.2	303.8	307.0	3.40
	4.3	300.00	317.8	303.9	309.3	4.50
	6.4	300.00	315.1	303.8	307.8	3.67
	8.6	300.00	313.9	303.7	307.1	3.32
	12.9	300.00	313.1	303.7	306.7	3.06

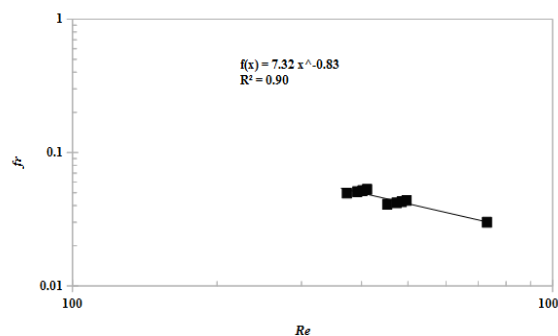


Fig. 6 Re versus fr

Table 4 Results of  $R_{th}$  and  $R_{hy}$  for flow fields studied

Model	$\alpha$	$D_{h-ch}$ $\mu m$	$\Delta p$ kPa	$R_{th}$ C/W	$R_{hy} * 10^{10}$ Pa s/m <sup>3</sup>
Present Work	4.3	81.13	206.84	0.21	9.12
	6.4	86.48	206.84	0.17	5.96
	8.6	89.58	206.84	0.15	4.33
	12.9	92.80	206.84	0.14	2.81
	4.3	81.13	300.00	0.18	7.54
	6.4	86.48	300.00	0.15	4.87
	8.6	89.58	300.00	0.13	3.52
	12.9	92.80	300.00	0.12	2.29
[20]	6.4	98.6	206.84	0.0898	1.88

It provides a basis for comparing hydraulic characteristics of flow-fields and fin geometries, Table 4.  $W_p$  is the product of volume flow rate and applied

$\Delta p$ . With branching,  $\Delta p$  increases due to secondary flows and increase in surface area, but shorter path lengths negate this effect of higher branching in flows. Higher  $\alpha$  for the same pitch, is a reason for increase in  $W_p$  as shown in Table 5. The convergent inlets act as a nozzle, increasing flow velocity, while the divergent outlet acts as a diffuser, improving pressure recovery at the exit to the flow field. The Re versus fr chart is shown in Fig. 6.

Table 5 Results of  $W_p$  and Nu evaluated at inlet for the flow fields studied

$\alpha$	$\Delta p$ kPa	$Re_{ch}$	fr	Q MW/m <sup>2</sup>	P.P W	PF 1/K	$Nu_{avg}$
4.3	206.84	372.9	0.049	0.5	0.54	9.43	17.79
6.4[20]	206.84	730	0.03	7.9	2.27	4.89	16.88
4.3	300.00	452.5	0.041	0.5	0.98	5.87	20.23
6.4	206.84	392.0	0.051	0.5	1.04	6.05	30.84
6.4	300.00	473.5	0.042	0.5	1.51	4.69	34.71
8.6	206.84	401.8	0.052	0.5	1.43	4.90	43.50
8.6	300.00	485.0	0.043	0.5	2.08	3.77	48.75
12.9	206.84	410.8	0.053	0.5	2.20	3.49	63.69
12.9	300.00	496.5	0.044	0.5	3.19	2.67	70.68

## 7. CONCLUSION

The following conclusions are based on the numerical analysis carried out in this work.

1. Bio-inspired flow field shows lower chip surface temperature variation than conventional flow fields.
2. At constant pressure inlet condition,  $R_{th}$  -0.126 C/W of the bio-inspired model is 1.4 times higher than the benchmark with channel  $D_h$ -92.8  $\mu$ m and is sufficient to cool latest processors like, AMD's 2990WX with a  $W_p$  consumption of 1.27% of, processor's TDP.
3. Aspect ratio-  $\alpha$  has significant impact on the hydro-thermal characteristics of finned heat sinks.
4. Higher aspect ratio and inlet pressure reduces the maximum base temperature and UCST value.
5. Higher aspect ratio increases  $Nu$  due to higher heat transfer area.
6. The correlation for all the flows analyzed in this work is given as;  $fr * Re^{0.83} = 7.32$  with  $R^2 = 0.90$ .

## REFERENCE

- [1] S. Lu and K. Vafai, A comparative analysis of innovative microchannel heat sinks for electronic cooling, *Int. Commun. Heat Mass Transf.*, 76, 2016, 271–284.
- [2] A. C. Kheirabadi and D. Groulx, Cooling of server electronics: A design review of existing technology, *Appl. Therm. Eng.*, 105, 2016, 622–638.
- [3] W. Qu and I. Mudawar, Experimental and numerical study of pressure drop and heat transfer in a single-phase micro-channel heat sink, *Int. J. Heat Mass Transf.*, 45(12), 2002, 2549–2565.
- [4] S. G. Kandlikar, High flux heat removal with microchannels-A roadmap of challenges and opportunities, *Heat Transf. Eng.*, 26(8), 2005, 5–14.
- [5] H. Wang, Z. Chen and J. Gao, Influence of Geometric Parameters on Flow and Heat Transfer Performance of Micro-Channel Heat Sinks, *Appl. Therm. Eng.*, 107, 2016, 870–879.
- [6] W. Escher, B. Michel and D. Poulikakos, Efficiency of optimized bifurcating tree-like and parallel microchannel networks in the cooling of electronics, *Int. J. Heat Mass Transf.*, 52(5–6), 2009, 1421–1430.
- [7] N. Guo, M. C. Leu, and U. O. Koylu, Bio-inspired flow field designs for polymer electrolyte membrane fuel cells, *Int. J. Hydrogen Energy*, 39, 2014, 21185–21195.
- [8] J. Currie, *Biomimetic design applied to the redesign of a PEM fuel cell*, M.A.Sc thesis, School of Mechanical and Industrial Engineering, University of Toronto, 2010.
- [9] R. Roshandel, F. Arbabi and G. K. Moghaddam, Simulation of an innovative flow- field design based on a bio inspired pattern for PEM fuel cells,” *Renew. Energy*, 41, 2012, 86–95.
- [10] D. Ouellette, A. Ozden, M. Ercelik, C. O. Colpan, H. Ganjehsarabi, X. Li and F. Hamdullahpur, Assessment of different bio-inspired flow fields for direct methanol fuel cells through 3D modeling and experimental studies, *Int. J. Hydrogen Energy*, 43(2), 2018, 1152–1170.
- [11] P. Trogadas, J. I. S. Cho, T. P. Neville, J. Marquis, B. Wu, D. J. L. Brett, and M. O. Coppens, A lung-inspired approach to scalable and robust fuel cell design, *Energy Environ. Sci.*, 11(1), 2018, pp. 136–143.
- [12] A. Arvay, J. French, J. C. Wang, X. H. Peng, and A. M. Kannan, Nature inspired flow field designs for proton exchange membrane fuel cell, *Int. J. Hydrogen Energy*, 38(9), 2013, 3717–3726.

- [13] F. Arbabi, Numerical Modeling of an Innovative Bipolar Plate Design Based on the Leaf Venation Patterns for PEM Fuel Cells, *Int. J. Eng.*, 25(3), 2012, 177–186.
- [14] M. Farzaneh, M. R. Salimpour and M. R. Tavakoli, Design of bifurcating microchannels with/ without loops for cooling of square-shaped electronic components, *Appl. Therm. Eng.*, 108, 2016, 581–595.
- [15] F. Cano-banda, C. U. Gonzalez-valle, S. Tarazona-cardenas and A. Hernandez-guerrero, Effect of different geometry flow pattern on heat sink performance, *12<sup>th</sup> Int. Con. Heat Tran., Fluid Mech. and Therm.*, Spain, 2016, 419–424.
- [16] X. Q. Wang, A. S. Mujumdar and C. Yap, Effect of bifurcation angle in tree-shaped microchannel networks, *J. Appl. Phys.*, 102(7), 2007, 073530.
- [17] <https://www.amd.com/en/products/cpu/amd-ryzen-threadripper-2990wx>, 2018.C.
- [18] COMSOL, *Introduction to COMSOL Multiphysics 5.3, Manual*, 2014.
- [19] D. Lorenzini-gutierrez, Variable Fin Density Flow Channels for Effective Cooling and Mitigation of Temperature Nonuniformity in Three-Dimensional Integrated Circuits,” *J. of Electronic Packaging.*, 136(2), 2014, 1–11.
- [20] D. B. Tuckerman and R. F. W. Pease, High-Performance Heat Sinking for VLSI, *IEEE Electron Device Lett.*, 5, 1981, 126–129.

$\Delta p$  -pressure drop  
 $\Delta T$  -temperature change

### Subscripts

avg -average values  
 b -base  
 ch -channel parameters  
 f -fluid properties  
 max -maximum  
 min -minimum  
 in -inlet parameters  
 out -outlet parameters  
 s -solid properties

### NOMENCLATURE

A -area  
 $D_h$  -hydraulic diameter  
 $f_r$  -channel friction factor  
 k -thermal conductivity  
 $P_o$  -Poiseuille number  
 PF -performance factor  
 $Q_{hy}$  -coolant flow rate  
 $Q_{th}$  -heat input to base plate  
 q -heat flux  
 $R_{th}$  -thermal resistance  
 $R_{hy}$  -hydraulic resistance  
 u -fluid velocity  
 T -local temperature  
 $W_p$  -pumping power

### Greek symbols

$\alpha$  -aspect ratio (height/width of channels)  
 $\alpha_{th}$  -coefficient of thermal expansion  
 $\rho$  -density  
 $\varepsilon$  -porosity  
 $\mu$  -dynamic viscosity